Finite Element Analysis of CM247LC Superalloy for Gas Turbine Blade Application

Tejan Chavan
Department of Mechanical Engineering, Symbiosis Institute of Technology, Pune, India
tejanchavan25@gmail.com

Nitin Khedkar
Department of Mechanical Engineering, Symbiosis Institute of Technology, Pune, India
nkkhedkar@gmail.com (corresponding author)

Received: 24 October 2024 | Revised: 21 November 2024 | Accepted: 27 November 2024

 DOI: https://doi.org/10.48084/etasr.9395

ABSTRACT

The objective of this article is to conduct a comparative analysis of the various materials used in the production of gas turbine blades. The materials under investigation include CM247LC, Nimonic 80A, and Inconel 738. The selected blade materials are required to demonstrate exceptional resistance to high temperatures and corrosion. It is determined that the most appropriate material for the construction of a gas turbine blade is a nickel-based superalloy. For the purposes of Finite Element Analysis (FEA), the aforementioned materials are defined as nickel-based superalloys. A comprehensive analysis of these materials was conducted using the ANSYS 2024 R2 student edition and a combination of structural and vibrational analyses was carried out. The deformation observed in CM247LC and Nimonic 80A exhibited nearly identical values of 0.965 mm and 0.884 mm, respectively. The results of the vibrational analysis indicated that all materials successfully circumvented the natural frequency as well as the operational natural frequency of 50 Hz, thereby ensuring the safe operation of the gas turbine blade. The findings demonstrated that the CM247LC satisfied both criteria for material selection, making it the most suitable material for gas turbine blade applications when compared to alternative materials. This is due to its comparatively lower deformation despite experiencing a greater magnitude of centrifugal force.

Keywords-gas turbine blade; CM247LC material; finite element analysis

I. INTRODUCTION

Gas turbines are used extensively in the fields of power generation, aviation, and marine propulsion. A gas turbine operates in three distinct phases: compression, combustion, and expansion. The fuel is initially drawn into the gas turbine through the inlet and subsequently passed through the compressor. The objective of the compression phase is to elevate the air pressure and render it more reactive with the fuel in the subsequent combustion stage. Then, the compressed air enters the combustion chamber, where the fuel is also injected. In the chamber, the fuel is mixed with high-pressure air [1]. Subsequently, the fuel-air mixture is ignited using an appropriate ignition source. Combustion is initiated by the release of a substantial quantity of heat energy, which gives rise to high temperatures and pressures within the combustion gases. The objective of combustion is to transform the chemical energy stored in the fuel into thermal energy in the form of hot and high-pressure gases. A turbine blade represents a discrete component within a gas turbine engine. A series of aerofoil-shaped blades are arranged within a slot of a disc that is attached to a rotating shaft. The aerofoil-shaped blades are designed in such a way that the distance between them is maintained, thus ensuring a uniform acceleration of the fluid flow. The blades serve the function of extracting thermal energy from the fluid that flows rapidly between them under conditions of extreme temperature and pressure. Turbine engines operate at elevated temperatures, ranging from approximately 850 °C to 1,700 °C [2]. The selection of the appropriate materials for gas turbine blades is of significant importance due to the extreme thermal and mechanical stresses to which they are subjected. Superalloys, particularly those formulated with nickel, have been widely used due to their exceptional attributes at high thermal conditions [3]. Nimonic 80A is a nickel-based superalloy that is renowned for its high tensile strength and resistance to corrosion at elevated temperatures. As a consequence, it is an ideal material for use in a variety of high-stress environments, including the aerospace and automotive industries. Its properties can be enhanced through various plasma nitriding and boriding treatments, which improve its performance under specific conditions. However, these treatments do not significantly alter its oxidation resistance [4]. Inconel 738 is a nickel-based superalloy that is renowned for its exemplary mechanical properties and high-temperature stability, rendering it an optimal choice for utilization in gas turbines and other high-stress environments. Although Inconel 738 is highly regarded for its mechanical and thermal properties, the processing

techniques and conditions can have a significant impact on its performance [5]. Additive manufacturing, also known as 3D printing, is markedly transforming the production of gas turbine blades, enabling intricate geometric designs and reduced material wastage. The fabrication of prototypes of blades exhibiting superior quality is currently being conducted using methodologies, such as fused deposition modeling and rapid investment casting [6]. The primary objective of this study is to perform a structural and modal analysis, with the goal of selecting the optimal material based on the findings of both analyses.

II. METHODOLOGY

The selection of the material for analysis was based on the properties that enable it to withstand high temperatures and exhibit excellent oxidation resistance. Therefore, nickel-based superalloys are capable of exhibiting the same exceptional characteristics of high-temperature resistance and oxidation resistance [7]. The CM247LC, Nimonic 80A, and Inconel 738 are all examples of nickel-based superalloys. To perform a FEA on the selected material, the following steps were followed:

- The CAD model of the gas turbine blade was prepared in the CATIA V5 software.
- The geometry was imported into the ANSYS 2024 R2 student edition.
- A fine mesh was generated for analysis purposes.
- The boundary conditions for the structural and modal analyses were set.
- A centrifugal load was applied at the edge of the blade tip perpendicular to the x-axis of the turbine blade, and a thermal condition of 10,000 °C and a rotational velocity of 3,000 rpm were used. These conditions were applied for the structural analysis.
- For the modal analysis, the root of the blade was fixed, and a thermal condition of 10,000°C was applied while the blade tip was free of any loading. The corresponding default setting of six modes was analyzed.
  Ultimately, the results were generated by the ANSYS software and the corresponding images were captured and presented in this study.

III. CALCULATIONS

The centrifugal force acting on the blade is calculated [8] by:

$$F = m\omega^2 r \quad (1)$$

where m is the mass of materials, r is the radial distance from the root of the blade to the tip of the blade, and ω is the rotational speed of the blade. In this case, the radius is 0.225 m, the mass is equal to the density of the material times the volume of the blade, and the blade volume is 0.00302 m^3. The angular velocity is 314.159 rad/sec. The aforementioned values were employed in order to calculate the corresponding centrifugal forces. The operational natural frequency is calculated using:

$$1\ \text{RPM} = 1/60\ \text{Hz} \quad (2)$$

$$3000\ \text{RPM} = (1/60) \times 3000 = 50\ \text{Hz}.$$

For the structural analysis, the displacement, stiffness, and load are given:

$$[F] = [k]\{x\} \quad (3)$$

where $[F]$ is the load matrix, $[k]$ is the structural stiffness matrix, and $\{x\}$ is the Nodal displacement matrix. For the Modal Analysis it can be used:

$$[k]\{\Phi i\} = \omega_i^2\,[M]\,\{\Phi i\} \quad (4)$$

where $[k]$ is the stiffness matrix, $\{\Phi_i\}$ is the mode shape matrix, $[M]$ is the mass matrix, and ω_i is the natural frequency. By evaluating this equation at each discrete node, one can ascertain the approximate dynamics of the comprehensive model.

IV. FINITE ELEMENT ANALYSIS

FEA represents a sophisticated mathematical methodology used to model the behavior of an object under specified physical conditions. This computational simulation instrument is employed by researchers, engineers, and mathematicians to forecast the response of a product to various real-world forces, including thermal effects, vibrations, and fluid dynamics. FEA is implemented across a diverse array of research and product design endeavors, including:

- Enabling the generation of virtual representations of tangible assets for the analysis of various conditions and scenarios.
- The use of FEA plays a crucial role in the evaluation of safety.
- FEA may serve as a non-invasive methodology for examining the biomechanics of living systems and the impact of the mechanical forces upon them.
- It can be used to enhance the precision of designs while providing insight into potential shortcomings [9].

The utilization of FEA is of vital importance in the examination of gas turbine blades, as it enables the comprehension of their structural soundness and performance characteristics when confronted with a range of operational scenarios. Gas turbine blades are subjected to extreme temperatures, elevated pressures, and significant centrifugal forces, which necessitates the design and analytical assessment of the blades to ensure both efficiency and safety during operation. FEA is employed to replicate these operational conditions and forecast the dynamic behavior of turbine blades, thereby facilitating the optimization of their design parameters and the selection of the appropriate materials. Vibration analysis using FEA is instrumental in understanding the natural frequencies and mode shapes of turbine blades, which are crucial for preventing resonance and potential failure [10].

A. CAD Model

A Computer-Aided Design (CAD) model of a gas turbine blade is presented in Figure 1.

B. Material Properties

A structural and vibrational analysis of a gas turbine blade was conducted on the materials CM247LC, Nimonic 80A, and Inconel 738, along with the boundary conditions for structural analysis and the boundary conditions for modal analysis, and are displayed in Tables I, II and III, respectively.

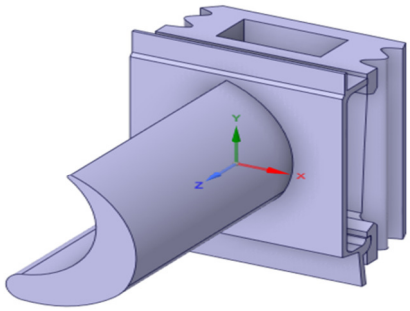

Fig. 1. CAD model of gas turbine blade.

TABLE I. PROPERTIES OF MATERIALS

Materials	Young's Modulus (GPa)	Density (kg/m^3)	Poisson's Ratio	Thermal Conductivity (W/m K)	References
CM247LC	197	9645	0.15	12	[11]
Nimonic 80A	222	8,190	0.35	11.2	[12]
Inconel 738	149	8,550	0.30	14.3	[13]

TABLE II. BOUNDARY CONDITIONS FOR STRUCTURAL ANALYSIS

Materials	Fixed Support	Loading End	Rotation Velocity (rad/sec)	Thermal Condition (^{0}C)	Force (kN)
CM247LC	The base of the blade is immobile.	End of the blade tip	314.159	1,000	646.830
Nimonic 80 A	The base of the blade is immobile.	End of the blade tip	314.159	1,000	549.253
Inconel 738	The base of the blade is immobile.	End of the blade tip	314.159	1,000	573.396

TABLE III. BOUNDARY CONDITIONS FOR VIBRATIONAL ANALYSIS

Materials	Fixed Support	No load applied	Rotational Velocity (rad/sec)	Thermal Condition (^{0}C)
CM247LC	The base of the blade is immobile	End of the blade tip is free	314.159	1,000
Nimonic 80 A	The base of the blade is immobile	Edge of the blade is free	314.159	1,000
Inconel 738	The base of the blade is immobile	Edge of the blade is free	314.159	1,000

V. RESULTS

A. Structural Analysis

Figure 2 shows the maximum deformation of the CM247LC material, which is indicated by the red color region. The corresponding value is 0.965 mm, and this occurs when a centrifugal force of 646.830 kN is applied. Figure 3 depicts the von Mises stress generated by the CM247LC material, which is 3622.3 MPa and is indicated by the red color region near the tip of the blade.

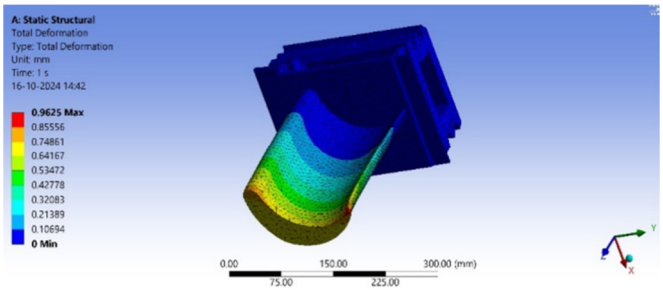

Fig. 2. Deformations of CM247LC material.

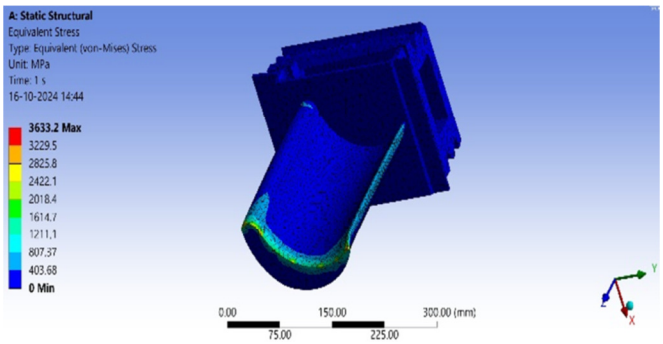

Fig. 3. Equivalent stress of CM247LC material.

As illustrated in Figure 4, the Nimonic 80A material is subjected to a centrifugal force of 549.253 KN, resulting in a maximum deformation of 0.884 mm. Figure 5 portrays the von Mises stress developed by the Nimonic 80A material, which reaches a maximum of 3019.6 MPa, while Figure 6 demonstrates that the Inconel 738 material exhibited the greatest deformation, reaching 1.389 mm, while subjected to a centrifugal force of 573.69 kN.

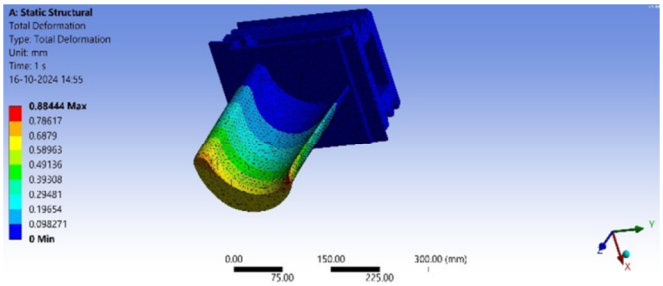

Fig. 4. Deformation of Nimonic 80A material.

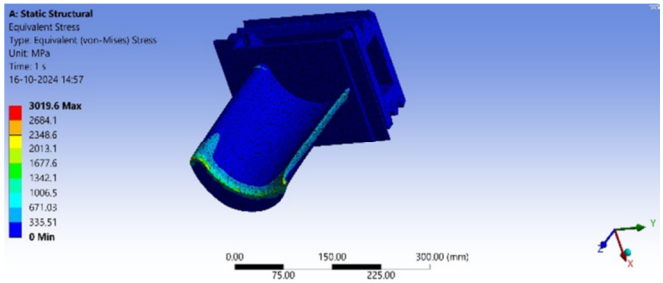

Fig. 5. Equivalent Stress of Nimonic 80A material.

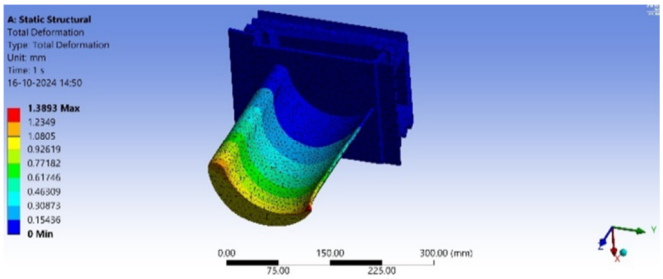

Fig. 6. Deformation of Inconel 738 material.

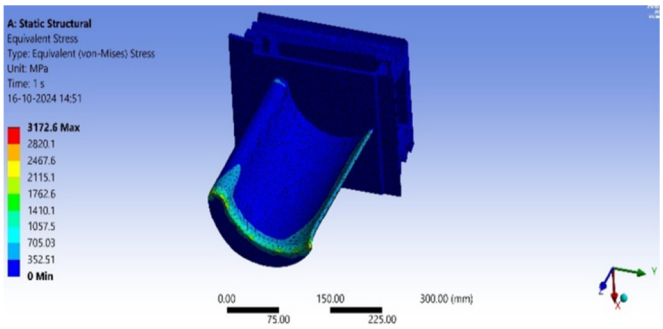

Fig. 7. Equivalent Stress of Inconel 738 material.

TABLE IV. RESULT TABLE FOR STRUCTURAL ANALYSIS

Materials	Equivalent (Von Mises) stress (MPa)	Total Deformation (mm)
CM247LC	3,633.2	0.965
Nimonic 80 A	3,019.6	0.884
Inconel 738	3,172.6	1.389

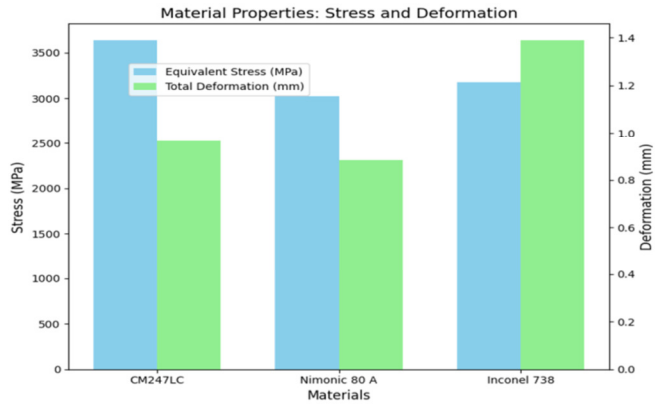

Fig. 8. Graph of Stress and Deformation for CM247LC, Nimonic 80A, and Inconel 738 material.

As displayed in Figure 7, the maximum value of the von Mises stress for the Inconel 738 material is 3172.6 MPa. All the above results are shown in Table IV and in Figure 8, where there is a graphical representation of the stress and deformation for all three materials.

B. Modal Analysis

Figures 9-14 present various modal shapes of the CM247LC material, in different deformations. Figures 15-20 show the variety of shapes and deformations for Nimonic 80A, while Figures 21-26 depict the modal shapes of Inconel 738 for different deformations.

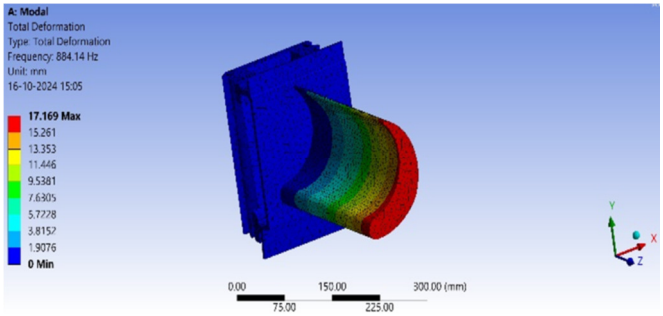

Fig. 9. Mode shape I of CM247LC material (deformation 17.169 mm).

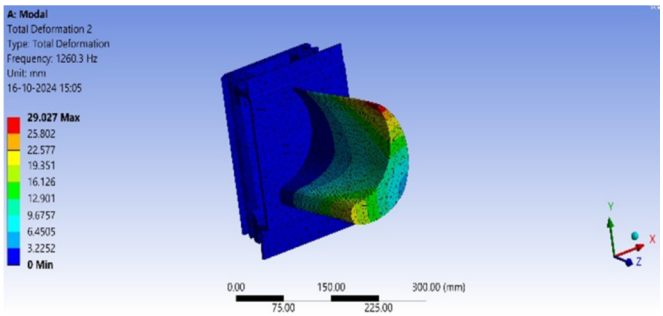

Fig. 10. Mode shape II of CM247LC material (deformation 29.027 mm).

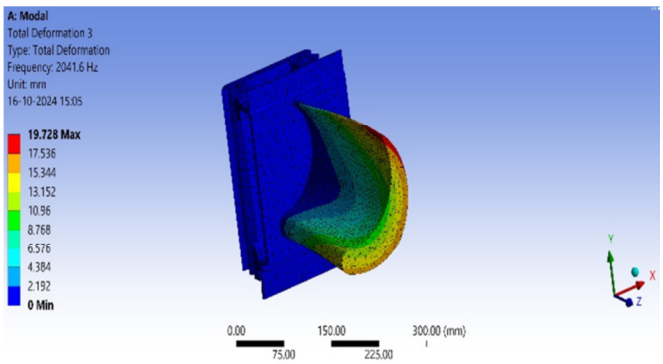

Fig. 11. Mode shape III of CM247LC material (deformation 19.728 mm).

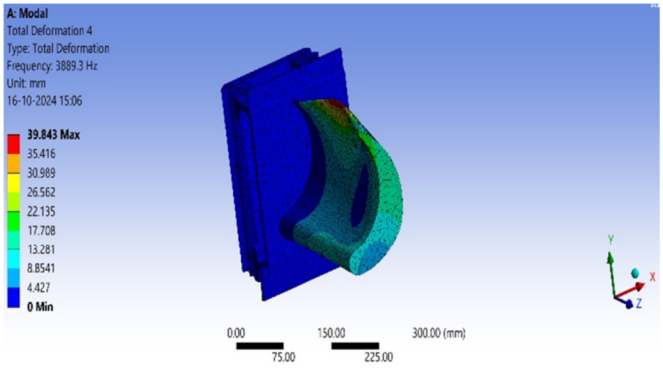

Fig. 12. Mode shape IV of CM247LC material (deformation 39.843 mm).

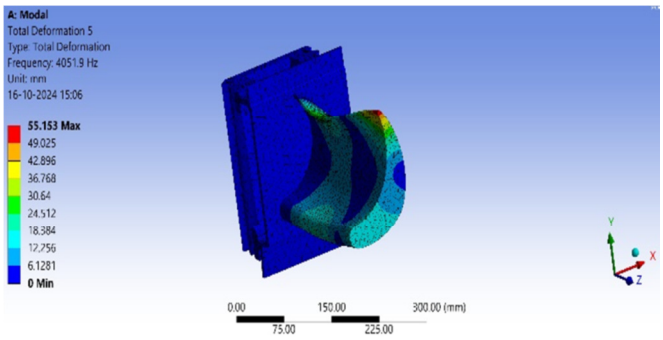

Fig. 13. Mode shape V of CM247LC material (deformation 55.153 mm).

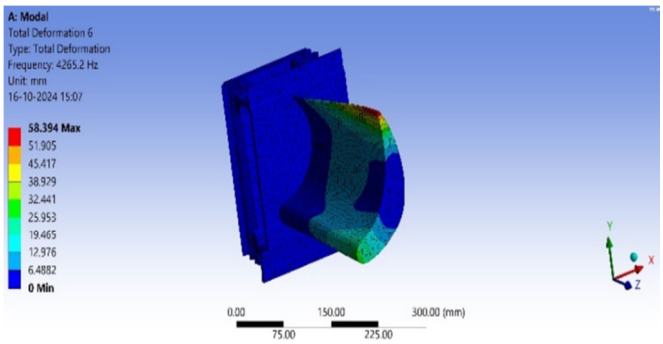

Fig. 14. Mode shape VI of CM247LC Material (deformation 58.394 mm).

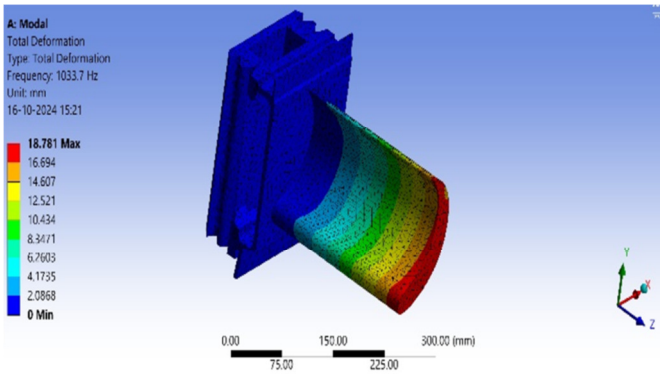

Fig. 15. Mode shape I of Nimonic 80A material (deformation 18.781 mm).

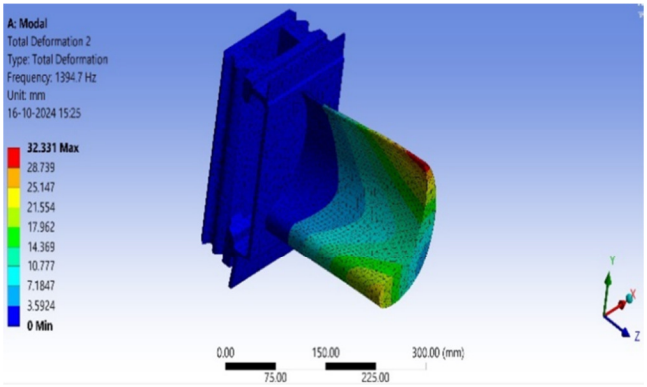

Fig. 16. Mode shape II of Nimonic 80A material (deformation 32.331 mm).

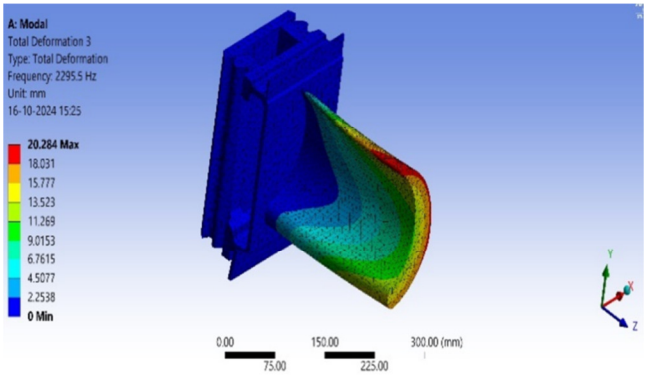

Fig. 17. Mode shape III of Nimonic 80A material (deformation 20.284 mm).

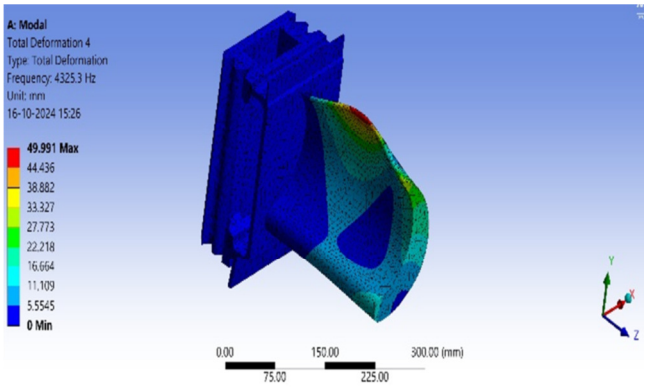

Fig. 18. Mode shape IV of Nimonic 80A material (deformation 49.991 mm).

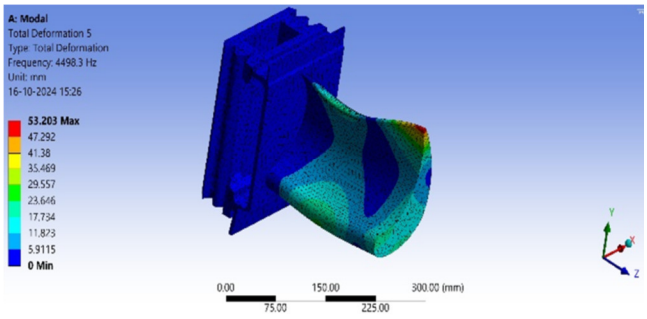

Fig. 19. Mode shape V of Nimonic 80A material (deformation 53.203 mm).

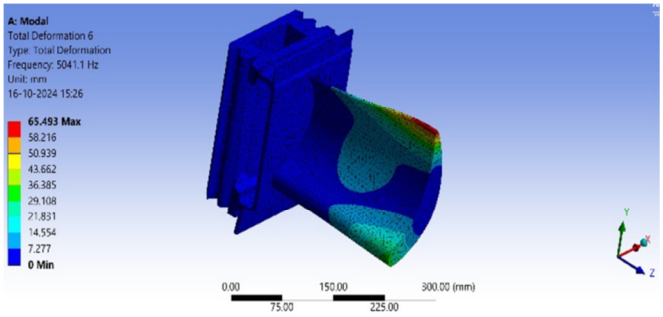

Fig. 20. Mode shape VI of Nimonic 80A Material (deformation 65.493 mm).

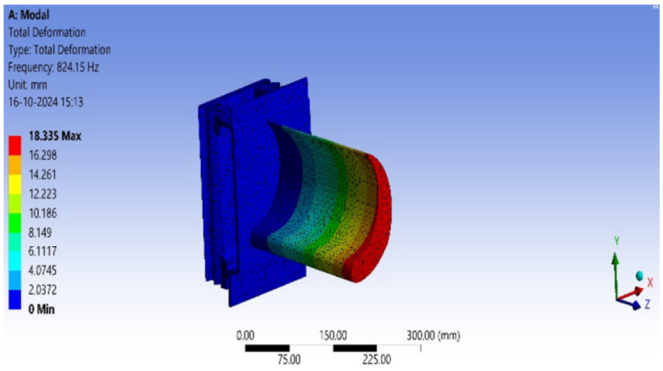

Fig. 21. Mode shape I of Inconel 738 Material (deformation 18.335 mm).

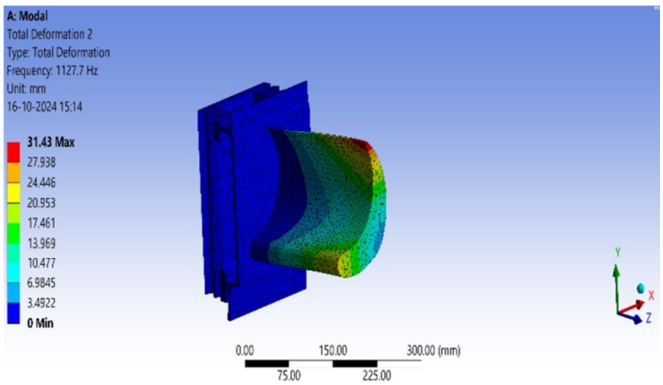

Fig. 22. Mode shape II of Inconel 738 Material (deformation 31.43 mm).

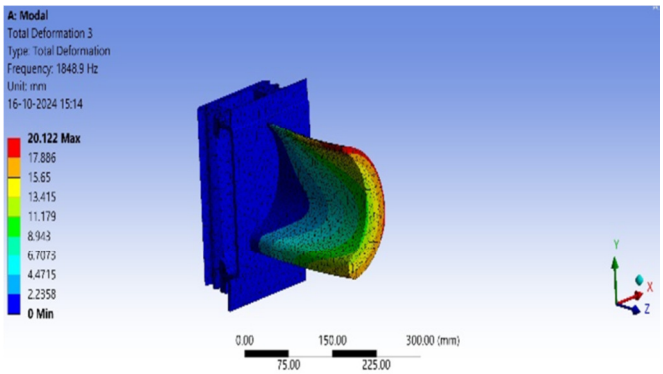

Fig. 23. Mode shape III of Inconel 738 Material (deformation 20.122 mm).

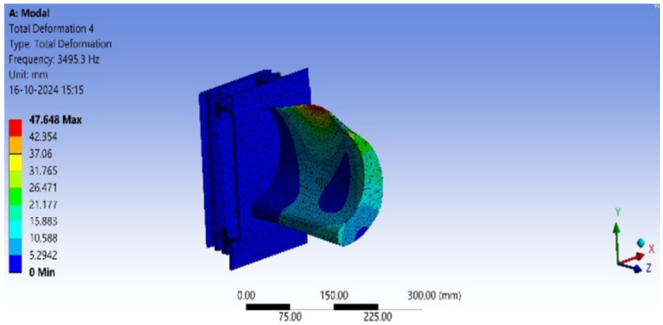

Fig. 24. Mode shape IV of Inconel 738 Material (deformation 47.648 mm).

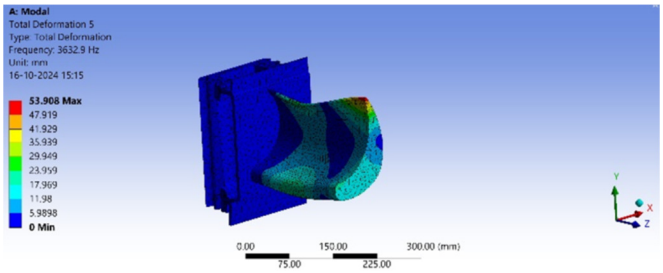

Fig. 25. Mode shape V of Inconel 738 Material (deformation 53.908 mm).

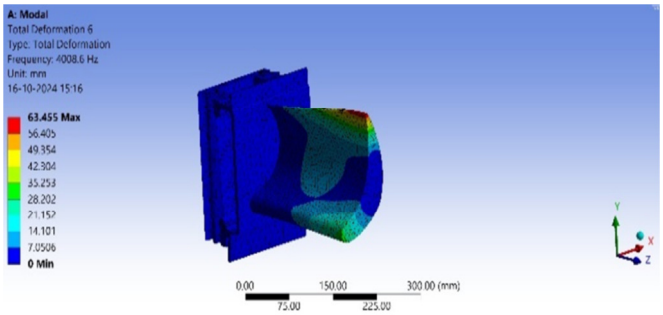

Fig. 26. Mode shape VI of Inconel 738 Material (deformation 63.455 mm).

Table V outlines the frequency range for the vibrational (modal) analysis.

TABLE V. FREQUENCY RANGE FOR VIBRATIONAL (MODAL) ANALYSIS

Mode Shapes	Frequency of Mode shapes (Hz)		
	CM247LC	Nimonic 80A	Inconel 738
I	884.14	1,033.7	824.15
II	1,260.3	1,394.7	1,127.7
III	2,041.6	2,295.5	1,848.9
IV	3,889.3	4,325.3	3,495.3
V	4,051.9	4,498.3	3,632.9
VI	4,265.2	5,041.1	4,008.6

VI. GRID INDEPENDENCE STUDY

Grid independence analyses, shown in Table VI, are of great significance in computational simulations, as they ensure that the outcomes remain unaffected by the specific arrangement of the numerical grid. This methodology includes the assessment of different grid resolutions to determine the point at which further refinement does not significantly impact

the results, thus certifying both precision and efficacy in simulations [14]. Figure 27 portrays the visual representation of the grid independence study. The graph outlines the deformation parameters for the CM247LC, Nimonic 80A, and Inconel 738 across a range of resolution values. From the data presented in the diagram, it can be surmised that as the resolution increases, the values demonstrate a convergence, which serves to indicate the successful achievement of grid independence.

VII. COMMENTS AND ANALYSIS

In the context of structural evaluation, it is observed that both deformation and the equivalent von Mises stresses reach their maximum values at the edge of the blade, while they reach their minimum values at the root or base of the blade. The modal analysis demonstrates a distinctive pattern of initiation of deformation at the tip of the blade (mode I) and subsequently progresses towards the edge of the blades (mode shape II and III), followed by bending modes in upward and downward directions (mode shape IV and V). The maximum deformation is demonstrated by mode shape VI. In the context of modal analysis, the CM247LC material exhibits a peak deformation of 58.394 mm at a frequency of 4,365.2 Hz, while the Nimonic 80A material demonstrates a peak deformation of 65.493 mm at a frequency of 5041.1 Hz. In contrast, the Inconel 738 material reveals a maximum deformation of 63.455 mm at a frequency of 4,008.6 Hz.

TABLE VI. GRID INDEPENDENCE STUDY OF DEFORMATION PARAMETER

Grid Resolution No.	**CM247LC**	**Nimonic 80 A**	**Inconel738**
	Deformation (mm)	Deformation (mm)	Deformation (mm)
1	0.93202	0.85229	1.3423
2	0.93914	0.86019	1.3532
3	0.94094	0.86318	1.3571
4	0.95444	0.87660	1.35774
5	0.95341	0.87596	1.3761
6	0.965	0.884	1.389

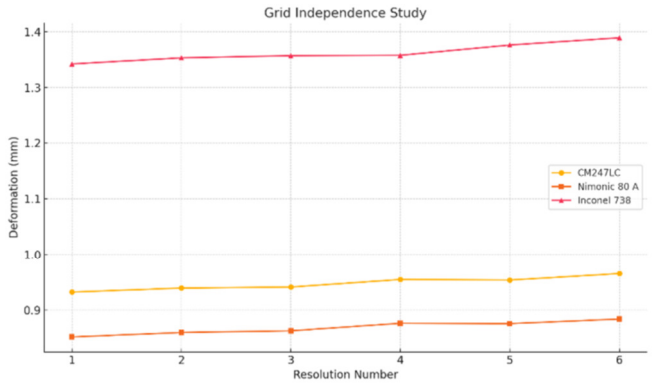

Fig. 27. Grid independence study of deformation parameter of CM247LC, Nimonic 80a, and Inconel 738.

VIII. DISSCUSSION

The material selection for the turbine blades should comply with the following criteria:

- The material should be capable of withstanding significant centrifugal forces and thermal loads with minimal deformation.
- The material should be designed to avoid critical or resonance frequencies, as well as operating frequencies, in order to ensure the safe operation of the gas turbine blades.

In consideration of the deformation characteristics, Inconel 738 exhibits a comparatively high degree of deformation in comparison to the other two materials. Accordingly, Inconel 738 is not deemed a viable option for the gas turbine blades when compared to CM247LC and Nimonic 80A materials, so, it fails to meet the first criterion. A comparison of the deformation values of CM247LC and Nimonic 80A reveals that they are nearly equal, given that the magnitude of the centrifugal force acting on CM247LC is significantly larger and its deformation is less pronounced. It can thus be concluded that the most suitable material for a gas turbine blade is CM247LC as it meets the initial criterion. Furthermore, the CM247LC material was found to avoid both the critical and resonance frequencies, as well as the operational frequency of 50 Hz. This demonstrates that the CM247LC material meets the second criteria.

IX. CONCLUSIONS

In this study, a comprehensive structural and vibrational analysis was conducted under thermal conditions of 10,000 °C and centrifugal forces acting on the blade edge with a rotational speed of 3,000 rpm. The resulting deformation and frequency range data were subjected to rigorous analysis. All the materials successfully avoided the critical frequency range of 200 Hz-300 Hz, thereby ensuring the safe operation of the gas turbine blade [15]. The CM247LC material satisfied both criteria for the material selection. Previous studies in the same area indicated that Nimonic 80A and Inconel 738 are suitable materials for turbine blade application. This research further attempts to identify new candidate materials for gas turbine blade application by comparing them with the best available materials. The CM247LC has been identified as a more suitable material for use in gas turbine blades. The Finite Element Analysis (FEA) analysis, in conjunction with the high-temperature strength and corrosion resistance properties of the CM247LC material, renders it a suitable candidate material for use in gas turbine blades, followed by Nimonic 80A and Inconel 738.

ACKNOWLEDGEMENT

The authors express their gratitude to the Management of Symbiosis International Deemed University Pune for providing the essential funding for the publication of this work.

REFERENCES

[1] M. Saraireh, "Heat Transfer Rate and Fluid Flow Analysis with Design Parameters of Gas Turbine using Beta-clog2-LSTM," *Engineering, Technology & Applied Science Research*, vol. 14, no. 5, pp. 16281–16289, Oct. 2024, https://doi.org/10.48084/etasr.8152.

[2] C. Verde and M. Sánchez-Parra, "Monitorability Analysis for a Gas Turbine Using Structural Analysis," *IFAC Proceedings Volumes*, vol. 39, no. 13, pp. 675–680, Jan. 2006, https://doi.org/10.3182/20060829-4-CN-2909.00112.

[3] R. Prabhakaran, "Jet Engine Gas Turbine Blades: Beyond the Super Alloys," *Journal of Aerospace Sciences and Technologies*, pp. 313–328, 2018, https://doi.org/10.61653/joast.v70i4.2018.393.

[4] P. Dziarski and N. Makuch, "The importance of plasma paste boriding parameters for thickness, nanomechanical properties, residual stress distribution and fracture toughness of layers produced on Nimonic 80A-alloy," *Engineering Fracture Mechanics*, vol. 275, Nov. 2022, Art. no. 108842, https://doi.org/10.1016/j.engfracmech.2022.108842.

[5] O. Ogunbiyi, S. Salifu, R. Sadiku, T. Jamiru, O. Adesina, and O. S. Adesina, "Influence of sintering temperature on microstructure and mechanical properties of graphene-reinforced Inconel 738 LC composites," *Materials Today: Proceedings*, vol. 38, pp. 743–748, Jan. 2021, https://doi.org/10.1016/j.matpr.2020.04.192.

[6] A. Sinha *et al.*, "A Review on the Processing of Aero-Turbine Blade Using 3D Print Techniques," *Journal of Manufacturing and Materials Processing*, vol. 6, no. 1, Feb. 2022, Art. no. 16, https://doi.org/10.3390/jmmp6010016.

[7] G. Chintala and P. Gudimetla, "Optimum Material Evaluation for Gas Turbine Blade Using Reverse Engineering (RE) and FEA," *Procedia Engineering*, vol. 97, pp. 1332–1340, Jan. 2014, https://doi.org/10.1016/j.proeng.2014.12.413.

[8] A. D. Antony, M. Gopalsamy, C. B. V. Viswanadh, and R. Krishnaraj, "Structural dynamic analysis of turbine blade," *IOP Conference Series: Materials Science and Engineering*, vol. 247, no. 1, Oct. 2017, Art. no. 012007, https://doi.org/10.1088/1757-899X/247/1/012007.

[9] T. Fadiji, C. J. Coetzee, T. M. Berry, A. Ambaw, and U. L. Opara, "The efficacy of finite element analysis (FEA) as a design tool for food packaging: A review," *Biosystems Engineering*, vol. 174, pp. 20–40, Oct. 2018, https://doi.org/10.1016/j.biosystemseng.2018.06.015.

[10] Kr. M. Salman and A. A. Khan, "Vibration Analysis of Turbine Blade Using Finite Element Method," in *Vibration Engineering and Technology of Machinery, Volume II*, Singapore, 2024, pp. 93–113, https://doi.org/10.1007/978-981-99-8986-7_7.

[11] R. Rajendran, V. Petley, and B. Rehmer, "Dynamic elastic properties of aero-engine metallic isotropic materials," *Proceedings of the Institution of Mechanical Engineers, Part L: Journal of Materials: Design and Applications*, vol. 227, no. 3, pp. 243–249, Jul. 2013, https://doi.org/10.1177/1464420712454071.

[12] H. P. Singh, A. Rawat, A. R. Manral, and P. Kumar, "Computational analysis of a gas turbine blade with different materials," *Materials Today: Proceedings*, vol. 44, pp. 63–69, Jan. 2021, https://doi.org/10.1016/j.matpr.2020.06.486.

[13] O. E. Efe-ononeme, A. Ikpe, and G. O. Ariavie, "Modal Analysis of Conventional Gas Turbine Blade Materials (Udimet 500 and IN738) For Industrial Applications," *Journal of Engineering Technology and Applied Sciences*, vol. 3, no. 2, pp. 119–133, Aug. 2018, https://doi.org/10.30931/jetas.452857.

[14] H. C. Siek, A. S. A. Kader, and C. L. Siow, "Grid independence study of low speed catamaran operate in shallow water," *AIP Conference Proceedings*, vol. 2484, no. 1, Mar. 2023, Art. no. 020003, https://doi.org/10.1063/5.0111116.

[15] M. P. Boyce, *Gas Turbine Engineering Handbook*, 4th ed. Oxford, UK: Butterworth-Heinemann, 2011.

[16] H.-E. Huang and C.-H. Koo, "Characteristics and Mechanical Properties of Polycrystalline CM 247 LC Superalloy Casting," *Materials Transactions*, vol. 45, no. 2, pp. 562–568, 2004, https://doi.org/10.2320/matertrans.45.562.